

Extremely Red Quasars from SDSS, BOSS and WISE: Classification of Optical Spectra

Nicholas P. Ross^{1,2*}, Fred Hamann³, Nadia L. Zakamska⁴, Gordon T. Richards^{2,5},
Carolyn Villforth^{3,6}, Michael A. Strauss⁷, Jenny E. Greene^{7,8}, Rachael Alexandroff⁴,
W. Niel Brandt^{9,10}, Guilin Liu⁴, Adam D. Myers^{11,5}, Isabelle Pâris¹²,
Donald P. Schneider^{9,10}

¹Lawrence Berkeley National Lab, 1 Cyclotron Road, Berkeley, CA 94720, USA

²Department of Physics, Drexel University, 3141 Chestnut Street, Philadelphia, PA 19104, USA

³Department of Astronomy, University of Florida, Gainesville, FL 32611-2055, USA

⁴Department of Physics & Astronomy, Johns Hopkins University, 3400 N. Charles St., Baltimore, MD 21218, USA

⁵Max-Planck-Institut für Astronomie, Königstuhl 17, D-69117 Heidelberg, Germany

⁶SUPA, School of Physics and Astronomy, University of St Andrews, North Haugh, St Andrews, KY16 9SS, UK

⁷Department of Astrophysical Sciences, Princeton University, Princeton, NJ 08544, USA

⁸Alfred P. Sloan Fellow

⁹Department of Astronomy and Astrophysics, The Pennsylvania State University, University Park, PA 16802, USA

¹⁰Institute for Gravitation and the Cosmos, The Pennsylvania State University, University Park, PA 16802, USA

¹¹Department of Physics and Astronomy, University of Wyoming, Laramie WY 82071, USA

¹²INAF - Osservatorio Astronomico di Trieste, Via G. B. Tiepolo 11, I-34131 Trieste, Italy

10 December 2018

ABSTRACT

Quasars with extremely red colours are an interesting population that can test ideas about quasar evolution as well as orientation and geometric effects in the so-called AGN unified model. To identify such a population we search the quasar catalogs of the Sloan Digital Sky Survey (SDSS), the Baryon Oscillation Spectroscopic Survey (BOSS) and the Wide-Field Infrared Survey Explorer (WISE) for quasars with extremely high infrared-to-optical ratios. We identify 65 objects with $r_{\text{AB}} - W4_{\text{Vega}} > 14$ mag (i.e., $F_{\nu}(22\mu\text{m})/F_{\nu}(r) \gtrsim 1000$). This sample spans a redshift range of $0.28 < z < 4.36$ with a median of $z \sim 1.5$ and includes three $z > 2.6$ objects that are detected in the $W4$ -band but not $W1$ or $W2$ (i.e., “ $W1W2$ -dropouts”). The SDSS/BOSS spectra show that the majority of the objects are reddened Type 1 quasars, Type 2 quasars (both at low and high redshift) or objects with deep low-ionization broad absorption lines (BALs) that suppress the observed r -band flux. In addition, we identify a class of Type 1 permitted broad-emission line objects at $z \simeq 2 - 3$ which are characterized by emission line rest-frame equivalent widths (REWs) of $\gtrsim 150\text{\AA}$ not characteristic of typical quasars. For example, 55% (45%) of the non-BAL Type 1s with measurable CIV in our sample have $\text{REW}(\text{CIV}) > 100$ (150) \AA , compared to only 5.8% (1.3%) for non-BAL quasars generally in BOSS. These objects often also have unusual line properties including unusually high $\text{N V}/\text{Ly}\alpha$ ratios. These large REWs might be caused by suppressed continuum emission analogous to Type 2 quasars; however, there is no obvious mechanism in the Unified Model to suppress the continuum without also obscuring the broad emission lines.

Key words: Astronomical data bases: surveys – Quasars: general – galaxies: evolution – galaxies: infrared.

1 INTRODUCTION

Quasars are the most luminous non-transient objects in the Universe, with L_{bol} reaching $\sim 10^{47-48}$ erg s^{-1} , powered by

* email: npross@physics.drexel.edu

accretion of matter onto supermassive black holes. To explain how quasars are fueled and become active, models (e.g., Sanders et al. 1988; Hopkins et al. 2005, 2006) suggest that mergers between gas-rich galaxies drive gas to the nuclei of merging galaxies, producing starbursts. The same activity fuels the growth of the supermassive black holes, which actively accrete matter at this stage, with much of the black hole growth happening in this ultra-violet (UV) and optically obscured phase. Feedback, potentially from a radiation-driven quasar wind, leads to removal of gas and dust from the central region, allowing the quasar to be seen in the UV and optical. These major-merger models are invoked to explain the obscuration/reddening observations noted in e.g., Urrutia et al. (2008), Glikman et al. (2012), and while they provide a reasonable fit to the observed quasar luminosity function (Richards et al. 2006b; Hopkins et al. 2007; Ross et al. 2013) and to clustering (e.g. Lidz et al. 2006; Myers et al. 2006, 2007; Ross et al. 2009; Shen et al. 2009; Shen 2009; White et al. 2012), there is little direct evidence for this picture in the form of a direct relationship between quasar activity and various stages in the galaxy interaction process (see e.g., Alexander & Hickox 2012; Fabian 2012; Heckman & Best 2014, for reviews).

Quasars appear with a wide range of observational properties. Intrinsically luminous quasars may or may not appear bright at optical, ultra-violet and X-ray wavelengths. Much of this variance can be explained in the context of the geometry-based ‘unification models’ (Antonucci 1993). If gas and dust are present near the active nucleus but do not completely surround it, then some lines of sight to the nucleus are clear, whereas others are blocked. In the former case, the observer can directly view the emission from the accretion disk, with the quasar appearing bright at X-ray, ultra-violet and optical wavelengths and displaying broad (several thousand km s^{-1}) emission lines in the optical spectra. These objects are termed unobscured, or Type 1, active nuclei (Khachikian & Weedman 1974). This contrasts with the situation where the observer’s line of sight is blocked by circumnuclear clouds; in this case X-rays are absorbed by the intervening gas and ultra-violet and optical photons are scattered and absorbed by the intervening dust. At optical wavelengths, often the only signature of nuclear activity in this case is strong, narrow emission lines produced in the material illuminated by the quasar along unobscured directions. These objects with weak ultra-violet and optical continua and narrow emission lines are designated Type 2 (or obscured) sources (Antonucci & Miller 1985; Smith et al. 2002; Zakamska et al. 2003; Brandt & Hasinger 2005; Reyes et al. 2008). Thus, obscuration, as part of an evolutionary phase or an orientation effect, is critical in determining the observed properties of quasars. However, because of their faintness at rest-frame optical and ultra-violet wavelengths, identifying Type 2 objects at high redshifts – at the peak of quasar activity $z \sim 2$ – remains challenging (Stern et al. 2002; Norman et al. 2002; Alexandroff et al. 2013; Greene et al. 2014).

The circumnuclear clouds of gas and dust absorb X-ray, ultra-violet and optical radiation from the quasar and re-emit this energy thermally at infrared wavelengths. This is why Type 1 quasars have similar luminosities at near- and mid-infrared wavelengths ($\sim 2 - 30\mu\text{m}$ in the rest-frame) as they do in the optical and in the ultra-violet (Elvis et al.

1994; Richards et al. 2006a; Polletta et al. 2008; Elvis 2010). Extremely obscured and dusty objects, in which optical emission is blocked, are therefore expected to show much higher infrared-to-optical ratios than Type 1 quasars. Indeed, a host of previous studies have used a *K*-band excess selection (Chiu et al. 2007; Maddox et al. 2008; Jurek et al. 2008; Nakos et al. 2009; Souchay et al. 2009; Wu & Jia 2010; Peth et al. 2011; Wu et al. 2011; Maddox et al. 2012; Fynbo et al. 2013; Wu et al. 2013), a near-infrared+radio selection (Glikman et al. 2004, 2007, 2012, 2013) or a mid-infrared selection (Lacy et al. 2004; Stern et al. 2005; Martínez-Sansigre et al. 2006; Richards et al. 2009; Donley et al. 2012; Stern et al. 2012; Banerji et al. 2013; Assef et al. 2013) to identify obscured (as well as unobscured) AGN.

In this paper, we describe a search for extremely red quasars to study the nature of the obscuration and the physical properties of quasars that have the unique orientations or evolutionary status that lead to these colours. We use optical photometry and spectroscopy from the Sloan Digital Sky Survey (SDSS; York et al. 2000) and SDSS-III (Eisenstein et al. 2011) Baryon Oscillation Spectroscopic Survey (BOSS; Dawson et al. 2013) as well as mid-infrared photometry from the Wide-Field Infrared Survey Explorer (WISE; Wright et al. 2010).

A second paper (Ross et al. 2014b; hereafter ‘Paper II’) describes the matched SDSS/BOSS+WISE quasar catalog in more detail (including the optical and mid-infrared colour-distributions, and radio properties of the sample) while a third paper (Hamann et al. 2014) presents a detailed investigation into a new class of objects, the extreme rest-frame equivalent width quasars, which are introduced here.

This paper is organized as follows. In Section 2, we describe our datasets and sample selection, and in Section 3 we present the basis sample properties of the extremely red quasars. In Section 4 we discuss the optical spectra of the extremely red quasars, classifying objects along the traditional lines of broad-line Type 1s, narrow-line Type 2s and those with interesting absorption features. In Section 4.8, we introduce the new class of extreme equivalent width quasars. We conclude in Section 5.

2 DATA AND SAMPLE SELECTION

2.1 Parent dataset

Our starting point is the spectroscopic quasar catalogs of the SDSS Seventh Data Release (DR7Q; Schneider et al. 2010; Shen et al. 2011) and the SDSS-III Tenth Data Release (DR10Q; Pâris et al. 2014). SDSS quasar targets were selected to have $i \leq 19.1$ if the colours were consistent with being at redshift $z \lesssim 3$, and $i \leq 20.2$ if $z \gtrsim 3$, as outlined in Richards et al. (2002). BOSS quasar targets are selected to a magnitude limit of $g \leq 22.0$ or $r \leq 21.85$, with the primary goal to select quasars in the redshift range $2.2 \leq z \leq 3.5$ as described in detail by Ross et al. (2012, and references therein). In both SDSS and BOSS, quasar targets are also selected if they are matched within $2''$ ($1''$ in the case of BOSS) of an object in the Faint Images of the Radio Sky at Twenty-cm (FIRST) catalog of radio sources (Becker et al.

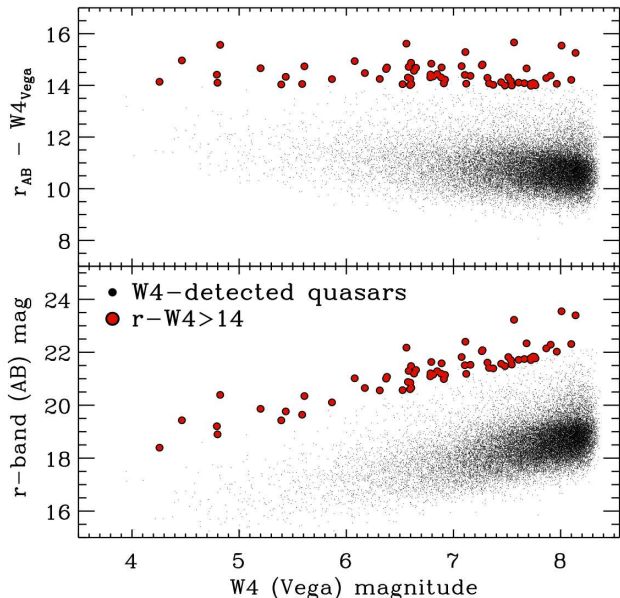


Figure 1. *Top:* $r - W4$ colour of the $W4$ -detected SDSS/BOSS quasars (black dots) as a function of $W4$ (i.e., $22\mu\text{m}$) magnitude. The quasars with $r - W4 > 14$ are shown as large red circles. *Bottom:* The r_{AB} -band magnitude versus $W4$. As a guide, $W4_{\text{Vega}} = 8.0$ mag corresponds to $W4_{\text{AB}} = 14.6$, or a flux density of $F_{\nu} \approx 6\text{mJy}$ (Wright et al. 2010).

1995). Both the SDSS DR7Q and BOSS DR10Q include quasars that were selected by algorithms other than the main quasar selections; these sources appear in the catalog due to being a ‘serendipitous’ (in SDSS, Stoughton et al. 2002) or an ‘ancillary’ (in BOSS, Dawson et al. 2013) target.

Luminous distant quasars are expected to be unresolved in optical ground-based observations, so we use point-spread function (PSF) magnitudes reported in the SDSS DR7 and BOSS DR10 quasar catalogs, corrected for Galactic extinction (Schlegel et al. 1998). Using the 2.5m Sloan telescope (Gunn et al. 2006), imaging data (Gunn et al. 1998) and spectra were obtained with the double-armed SDSS/BOSS spectrographs which have $R = \lambda/\text{FWHM} \sim 2000$ (Smee et al. 2013). Redshifts are measured from the spectra using the methods described in Bolton et al. (2012) and the data products are detailed in the SDSS DR7 (Abazajian et al. 2009) and DR10 (Ahn et al. 2014) papers.

The SDSS DR7 and BOSS DR10 quasar catalogs include 105,783 objects across 9380 deg^2 , and 166,583 objects across $6,370\text{ deg}^2$, respectively, with 16,420 objects in common to both catalogs. Thus our superset of optical data has 255,946 objects, and we use the BOSS spectrum (which has higher S/N and a larger wavelength coverage) when there are duplicate spectra between the two catalogs.

WISE mapped the sky in four filters centered at 3.4, 4.6, 12, and $22\mu\text{m}$ ($W1$, $W2$, $W3$, and $W4$ bands), achieving 5σ point-source sensitivities better than 0.08, 0.11, 1, and 6 mJy, respectively. The WISE Explanatory Supplement¹ provides further details about the astrometry and photometry in the source catalog. We retrieved photometric quantities

for each of the four WISE bands. Hereafter, we use the notation SNR_{W_x} for the signal-to-noise ratio and W_x for the Vega-based WISE magnitudes, in band $x = 1, 2, 3$ and 4.

Because of established conventions, we report Sloan Digital Sky Survey (SDSS) *ugriz* magnitudes on the AB zero-point system (Oke & Gunn 1983; Fukugita et al. 1996), while the Wide-Field Infrared Survey Explorer (WISE) $W1 - 4$ magnitudes are calibrated on the Vega system (Wright et al. 2010). For WISE bands, $m_{\text{AB}} = m_{\text{Vega}} + \Delta m$ where $\Delta m = (2.699, 3.339, 5.174, 6.620)$ for $W1$, $W2$, $W3$ and $W4$, respectively (Cutri et al. 2011). We make use of the Explanatory Supplement to the WISE All-Sky Data Release, as well as the WISE AllWISE Data Release Products online.

The WISE team has released two all sky catalogs: the 9 month cryogenic phase of the mission led to the WISE All-Sky (“AllSky”) Data Release; while the WISE AllWISE Data Release (“AllWISE”) combines the AllSky data with the NEOWISE program (Mainzer et al. 2011). The resulting AllWISE dataset is deeper in the two shorter WISE-bands (5σ point-source sensitivities now 0.054 and 0.071 mJy), and the data processing algorithms were improved in all four W -bands.

We match the sample of the 255,946 unique quasars in the SDSS DR7Q and BOSS DR10Q, and use both the All-Sky and the AllWISE data available at the NASA/IPAC Infrared Science Archive (IRSA)², with a matching radius of $2''$. For the combined DR7Q+DR10Q, we find 203,680 matches; 102,083 objects (96.5%) of the DR7Q and 111,779 (67%) of the DR10Q are matched in one or more WISE bands. The difference in the percentage of matches is expected since BOSS is fainter than SDSS. Matching with DR10Q positions offset in Right Ascension and Declination by of $6''$, $12''$ and $18''$ ($\sim 1, 2$ and 3 times the WISE angular resolution in $W1/2/3$) return, respectively, 508, 893 and 873 matches within $2''$, suggesting our false-positive matching rate is $\lesssim 1\%$ (see also Krawczyk et al. 2013).

With a matching radius of $2''$, 15,843 of the SDSS DR7 quasars, and 2,979 of the (optically fainter) BOSS DR10 quasars have a good match in the WISE $W4$ band, i.e., $\text{SNR}_{W4} \geq 3$, $W4 < 8.00$ (close to the nominal 5σ point source sensitivity of $W4 = 7.9$, Wright et al. 2010) and the WISE contamination and confusion flag, `cc_flags` set to “0000”, suggesting the source is unaffected by known artifacts in all four bands. Table 1 presents an overview of the numbers of SDSS/BOSS quasars in the WISE-matched dataset.

2.2 Extremely red quasar criterion

Motivated by the discovery of a population of $z \sim 2$, dust-obscured galaxies revealed by the *Spitzer* Space Telescope (Dey et al. 2008), we apply similar selection criteria to the SDSS/BOSS+WISE matched quasars; see Figure 1. In particular, we require the spectroscopic quasars to have a reliable detection in the WISE $W4$ -band:

$$\text{SNR}_{W4} \geq 3 \quad (1)$$

a colour of

$$r - W4 > 14.0 \quad (2)$$

¹ wise2.ipac.caltech.edu/docs/release/allwise/expsup/index.html

² mhttp://irsa.ipac.caltech.edu/

Description	Unique objects	from SDSS	from BOSS
DR7Q and DR10Q quasars ^a	255 946	105 783	166 583
+ matched to WISE	203 680	102 083	111 779
+ “good” $W4$ ^b	17 744	15 843	2 979
and $r - W4 > 14.00$	65	19	48

Table 1. Overview of the numbers of SDSS/BOSS quasars in the WISE-matched dataset. ^aThere are objects common to both SDSS DR7Q and BOSS DR10Q that have WISE matches. Hence, the sum of the “From SDSS” and “From BOSS” columns is greater than the given total. ^b“Good” $W4$ detections have $\text{SNR}_{W4} \geq 3$ and $W4 < 8.00$ and `cc_flags` eq “0000”.

i.e., $r_{\text{AB}} - W4_{\text{AB}} \gtrsim 7.5$, which corresponds to $F_{\nu}(22\mu\text{m})/F_{\nu}(r) \gtrsim 1000$, and

$$W4 \leq 8.00. \quad (3)$$

We further include objects with $W4 > 8.00$ if the object has $\text{SNR}_{W4} \geq 3$ and $W4 - \sigma_{W4} < 8.00$. In Table 1 we outline the stages in the selection and the resulting number of quasars after every step.

As dust around an AGN is expected to sublimate at a temperature of $\sim 2000\text{K}$, at high redshift our WISE $W4$ i.e., $22\mu\text{m}$ -based selection, is sensitive to hot dust since $W4$ probes $\lambda \simeq 7.3\mu\text{m}$ at $z \approx 2$ (Draine & Li 2007; Elitzur 2008; Diamond-Stanic & Rieke 2010). This is of particular interest because at these redshifts shorter wavebands (e.g. $W1$) may cease to trace dust emission at $z \approx 2$.

For the $W4$ selection we require $r - W4 > 14$ and has also been shown by the WISE team to locate Type 2 quasars at $z \sim 2$ (Wu et al. 2012; Yan et al. 2013).

Our selection applied to both the AllSky and AllWISE catalogs results in very similar samples, and any object that passes the criteria in equations (1)-(3) in either of these data releases is included. There are 65 quasars that have spectra from SDSS/BOSS and satisfy the extremely red criterion from the union between the two WISE datasets. The $W4$ PSF has a full width at half maximum (FWHM) of $12''$, much larger than the optical PSF, so a nearby galaxy and a quasar cannot be deblended in $W4$ observations if they are a few arcseconds apart.

We visually inspected the SDSS and WISE images of the 65 objects using the SDSS Image List Tool and the IRSA WISE Image Service, and establish that there is no other obvious optical source (down to the 5σ -depth of the SDSS photometric survey of $r = 22.7$) within $6''$ of our target. In only two cases there is potential concern that another optical object boosts the $W4$ flux - we return to this in Section 4.4. Also, although bright in $W1$ and $W2$, brown dwarfs tend to be significantly fainter than 8th magnitude in $W4$ (Kirkpatrick et al. 2011), so we do not suspect contamination from these objects. Overall, we consider all 65 $r - W4 > 14$ quasars good matches.

Name (SDSS J)	R.A. (J2000)	Decl. (J2000)	z	r -mag (AB)	W4 mag (Vega)	$r - W4$	$F_\nu[W4]$ / $F_\nu(r)$	Radio flux	REWs / \AA	FWHM / km s^{-1}	Notes	bitwise
0832000.2+1615000.3	128.00085	16.25011	2.423	21.82±0.08	7.51±0.16	14.31	1335	1.1	-	-	Type 1, EREW, strong associated absorption lines	1001 0001
011110.83+204543.8	17.79517	20.76218	2.432	22.03±0.09	7.96±0.21	14.06	1064	-	0±0	0±0	Ly- α emitter QSO	0000 0001
090630.73+082837.3	136.62806	8.47705	2.437	21.77±0.09	7.76±0.20	14.00	1009	22.8	3±1	340±159	Type 1 (from Ly- α width)	0001 0001
093638.41+101930.3	144.16006	10.32510	2.458	21.72±0.06	7.61±0.17	14.11	1110	-	169±4	1273±20	Type 2, but with EREW	1000 0010
134026.99+083427.2	205.11248	8.57424	2.490	22.31±0.13	8.10±0.21	14.21	1223	-	338±11	2088±51	Type 2, but with EREW	1000 0010
221524.00-005643.8	333.85003	-0.94550	2.493	22.29±0.12	7.91±0.24	14.38	1427	-	152±5	4226±112	EREW	1000 0001
111017.13+193012.5	167.57139	19.50347	2.497	20.61±0.03	6.59±0.07	14.01	1015	-	-	-	EREW	1000 0010
155102.79+084401.1	237.76163	8.73366	2.520	20.66±0.03	6.61±0.06	14.05	1054	2.9	10±3	2467±426	FeLoBAL	0011 0001
083448.48+015921.1	128.70202	1.98921	2.594	21.19±0.05	6.88±0.09	14.31	1337	-	214±7	2864±73	EREW, Type 2	1000 0010
220337.79+121955.3	330.90749	12.33204	2.626	21.57±0.05	7.45±0.14	14.12	1124	-	262±3	1072±10	EREW, Type 2	1000 0010
085124.78+314855.7	132.85329	31.81548	2.638	21.63±0.07	6.79±0.08	14.84	2180	-	76±5	3584±181	Type 1, W1W2-dropout	0100 0001
100424.88+122922.2	151.10370	12.48952	2.640	22.15±0.12	7.87±0.19	14.28	1303	12.3	-	-	FeLoBAL	0011 0001
104611.50+024351.6	161.54796	2.73103	2.772	21.51±0.07	7.11±0.11	14.40	1459	-	203±7	5181±144	Type 1, Nv/Ly α > 1, EREW	1000 0001
155434.17+110950.6	238.64238	11.16407	2.936	21.19±0.05	6.63±0.08	14.56	1688	-	-	-	BAL, probably FeLoBAL	0010 0001
135959.73+052512.3	209.99888	5.42008	3.055	22.08±0.11	7.27±0.09	14.81	2117	-	70±10	7250±833	W1W2-dropout	0100 0001
022052.11+013711.1	35.21715	1.61976	3.138	21.82±0.08	7.08±0.09	14.74	1995	-	341±19	2843±167	Type 1, W1W2-dropout	0100 0001
101439.51+413830.6	153.66466	41.64183	4.360	21.84±0.08	7.74±0.16	14.10	1097	-	118±8	13568±684	FeLoBAL	0010 0001

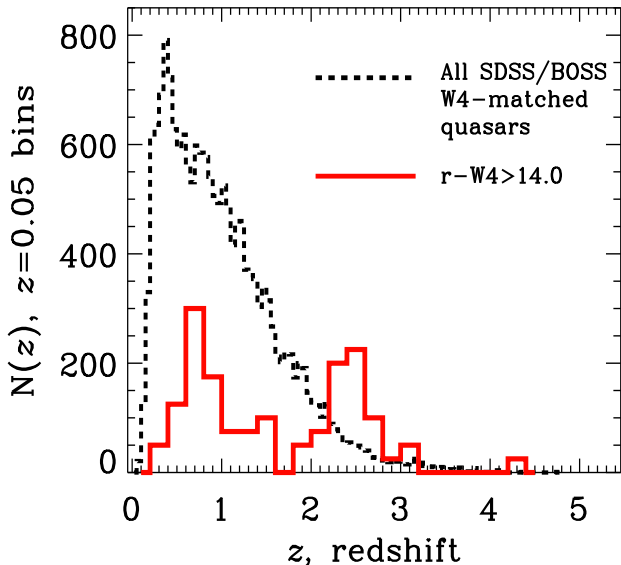


Figure 2. The redshift distribution of the 17,744 SDSS/BOSS quasars with good W4 matches is given by the black (dashed) histogram. The redshift distribution of extremely red quasars (with $r - W4 > 14$) is given by the solid (red) line. It has a binwidth of $z = 0.20$ and is renormalized to peak at 300. This maximum bin, at $z \approx 0.70$, actually has 12 objects.

3 KEY PROPERTIES OF THE EXTREMELY RED QUASARS

The key properties of the extremely red quasar sample are provided in Table 2: the catalog name of the object, its Right Ascension, Declination, redshift, magnitude and colour properties. The $W4$ flux density (in Jansky’s) is calculated directly from the $W4$ magnitude as prescribed by the WISE Explanatory Supplement. A power-law slope of $\alpha = 1$ and $F_\nu \propto \nu^{-\alpha}$ is assumed (Table 1 of Wright et al. 2010), but no attempts are made to compute an absolute $W4$ or r -band magnitude and thus no k -correction is employed. The Radio fluxes are the integrated flux densities (F_{int}) measured in mJy at 20cm from the FIRST survey (Becker et al. 1995). The Rest-frame Equivalent Widths (REWs) are given for Mg II at $z \leq 1.5$ and C IV for objects at redshift $z > 1.5$. The Full-Width, Half-Maximum (FWHM) of the relevant emission line is also quoted, with the REW and FWHM measurements coming from fits to the line profiles, as described in Hamann et al. in prep.

We give each object a classification based on optical spectral properties, indicated by the bitwise values described in Table 3. These classifications were all performed by visual inspection, with objects being assigned to the classes given in Table 3 depending on the presence (or absence) of broad/narrow emission lines, broad absorption features, the indications of ongoing or recently ceased star-formation, or objects with large equivalent width in the C IV emission line. These visual inspections are generally qualitative but as discussed in Section 4, aid us to understand the sample and physical types of quasar the $r - W4 > 14$ colour selects.

We also present a short note on each object in Table 2. Again, these notes are generally qualitative assessments based on visual inspection of the optical spectra. We do not

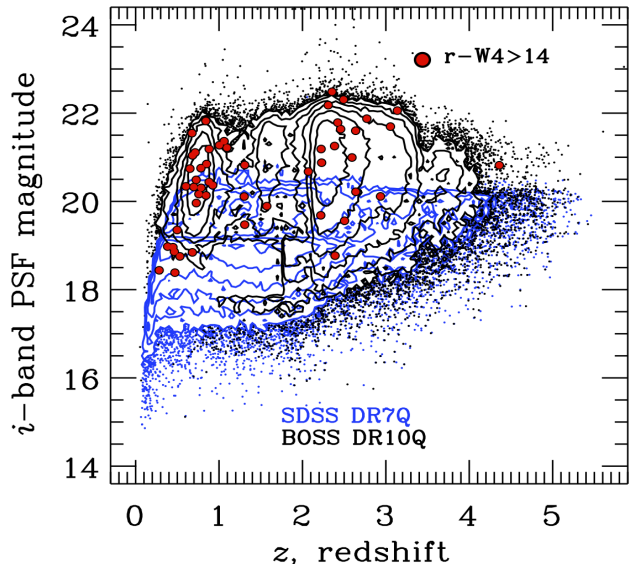


Figure 3. The redshift versus i -band magnitude distribution for the extremely red quasars satisfying the $r - W4 > 14$ selection. The blue and black contours show the distributions for the SDSS DR7 and the BOSS DR10 quasar catalogs, respectively.

quantify e.g. [O II] strength, but use these notes to make the link between the classifications given in Table 3 and the discussions presented in Section 4. We call a quasar “red” when its spectral slope is shallower than the Vanden Berk et al. (2001) template. The acronyms SB, RLQ and EREW stand for starburst, Radio Loud Quasar and Extreme Rest-frame Equivalent Width, the latter of which we introduce and describe in Section 4.8.

The redshift range for the extremely red quasars is $0.282 < z < 4.36$, and half the sample is fainter than $r=21.4$. Figure 2 shows the redshift distribution of the sample compared to the full redshift distribution of the 17,744 SDSS/BOSS quasars with good W4 matches. The redshift distribution of the $r - W4 > 14$ sample is bimodal, with peaks around $z \sim 0.8$ and $z \sim 2.5$. In Figure 3 the redshifts and i -band magnitudes are displayed for the $r - W4 > 14$ objects, and compared to the distributions from the full SDSS DR7 and BOSS DR10 quasar catalogs. SDSS quasars use the i -band for selection limits, so we use this further in this figure. One can identify the $i = 19.1$ magnitude limit contour for the SDSS $z \lesssim 2.5$ quasars, as well as the redshift histogram peaks at $z \sim 0.6 - 1.0$ and $z \sim 2.2 - 2.7$ seen in the BOSS quasar distribution (e.g. Fig. 2 in Pâris et al. 2014).

Figure 4 presents the magnitude-redshift relations for the SDSS/BOSS+WISE matched catalog, including objects with good $W4$ matches, and the extremely red sample, in the r and $W4$ -bands, as well as the distribution in redshift vs. $r - W4$ colour. This plot can be directly compared with Yan et al. (2013) (and their Figure 20). Yan et al. (2013) have also merged the WISE photometry with the SDSS (though not BOSS), and describe the spectroscopic observations of eight objects that have $r - W4 > 14$ (see their Table 1 for details). Although we have an order of magnitude more $r - W4 > 14$ objects at $z > 2$, the Yan et al. objects

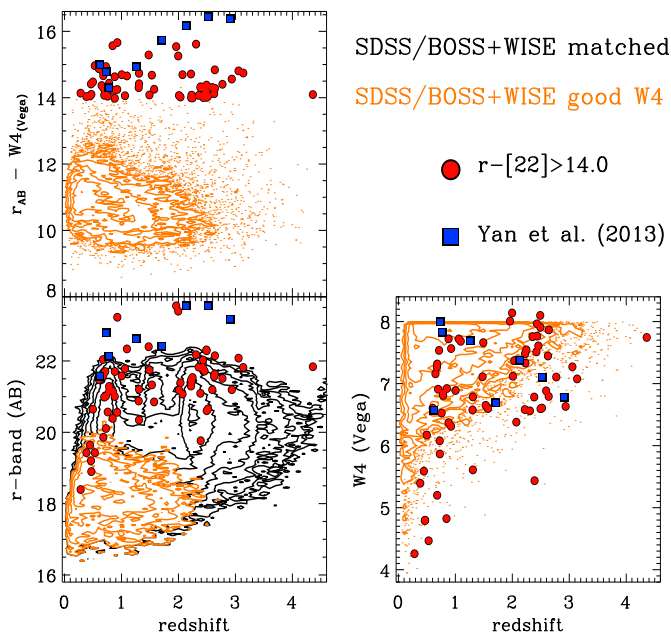


Figure 4. The magnitude-redshift and colour-redshift diagrams for the objects with a WISE match (black contours) and objects with a good $W4$ match (orange contours). The $r - W4 > 14$ extremely red quasar population are shown by the red circles. *Top left:* Redshift vs. $r - W4$ colour; *bottom left:* Redshift vs. r -band AB magnitude and *bottom right:* Redshift vs. $W4$ Vega magnitude. The data from Yan et al. (2013) are indicated by the blue squares.

General Description	Bitwise Value	Number in Sample
Type 1 QSO	0000 0001	36
Type 2 QSO	0000 0010	29
Starburst	0000 0100	5
post-starburst	0000 1000	2
Radio Loud	0001 0000	37
(Fe)LoBAL	0010 0000	10
W1W2-dropouts	0100 0000	3
“Extreme” REWs	1000 0000	12

Table 3. The classifications of the optical spectra of the extremely red quasar sample, the bitwise value associated with each classification and the number in the sample. Aside from the Type 1/Type 2 dichotomy, the categories are not mutually exclusive. Radio Loud is defined as $\mathcal{R} > 10$.

are significantly fainter in the optical than our SDSS/BOSS detected objects. Based on the spectral properties of the Yan et al. (2013) sample, 3/8 are classified as Type-1 AGN, 3 objects are Type-2 AGN, and the remaining two objects have features consistent with either a Type-2 AGN, or a star-forming galaxy, broadly in line with the composition given in Table 3.

4 CLASSIFICATIONS FROM OPTICAL SPECTROSCOPY

The spectra of the extremely red quasar sample are publicly available at the SDSS-III Science Archive Server³. The optical spectra can be classified into various groups (see Table 3). We broadly classify the objects that satisfy the $r - W4 > 14$ selection into: *(i)*: unobscured (but reddened) Type 1 quasars possessing broad lines (bitwise value 1 in Table 3); *(ii)*: objects that show evidence for being narrow-line Type 2 quasars from their optical spectra (bitwise value 2 in Table 3); *(iii)*: objects that suggest ongoing, or recently ceased star-formation (bitwise values 4 and 8); *(iv)*: quasars with blue-shifted absorption features (bitwise value 32); *(v)*: objects that are not detected in the WISE $W1/2$ -bands (bitwise 64) and *(vi)*: a class of Type 1 sources with extreme rest equivalent widths in their UV broad lines, namely, $\text{REW} > 150\text{\AA}$ in either C IV or Mg II. These classification groups are not mutually exclusive; several objects are assigned to multiple groups. These sources are indicated by the bitwise values in the last column of Tables 2, described in Table 3 and example spectra are presented below.

4.1 Type 1 Quasars

Figure 5 presents the spectra of six examples of extremely red quasars, classified as Type 1 based on their optical spectroscopy. We classify these objects as Type 1 quasars since objects in this class are observed to have broad emission lines typical of Type 1 quasars. Where measured, the mean line widths are $\text{FWHM}(\text{Mg II}) \sim 6440 \text{ km s}^{-1}$ and $\text{FWHM}(\text{C IV}) \sim 4900 \text{ km s}^{-1}$. Figure 5 lists the SDSS name, redshift, classification (from Table 3) and $r - W4$ colour.

The spectra in Figure 5 are heterogeneous; some show blue continua, while some are red. One object displays strong Fe II and the first object (with the lowest redshift in our sample) has unusually broad [O III] (see also section 4.4). Many of the examples of Type 1 quasars from our selection appear to be significantly reddened (Richards et al. 2003) often with a host galaxy component.

Glikman et al. (2013) identify dust-reddened quasars by matching the FIRST radio catalog to the UKIRT Infrared Deep Sky Survey (UKIDSS; Lawrence et al. 2007). This study identified 14 reddened quasars with $E(B - V) > 0.1$, including three at $z > 2$. However, Glikman et al. (2013) find no heavily reddened ($E(B - V) \gtrsim 0.5$) quasars at high redshifts ($z > 2$). The object ULASJ1234+0907 ($z = 2.503$) discovered by Banerji et al. (2014) is currently the reddest broad-line Type 1 quasar known, with $(i - K)_{\text{AB}} > 7.1$. Since all our extremely red quasar have $i \lesssim 22$ mag and a range of $1.62 < (i - K)_{\text{AB}} < 4.73$ (Paper II), none of our objects have optical-to-near infrared colours as red as ULASJ1234+0907.

4.2 Type 2 Quasar candidates at low redshift

We define Type 2 quasars as objects with narrow emission lines and that do not have an underlying broad component, and with line ratios characteristic of non-stellar ionizing radiation (Reyes et al. 2008). Specifically, in Type 2 quasars

³ <http://sas.sdss3.org>

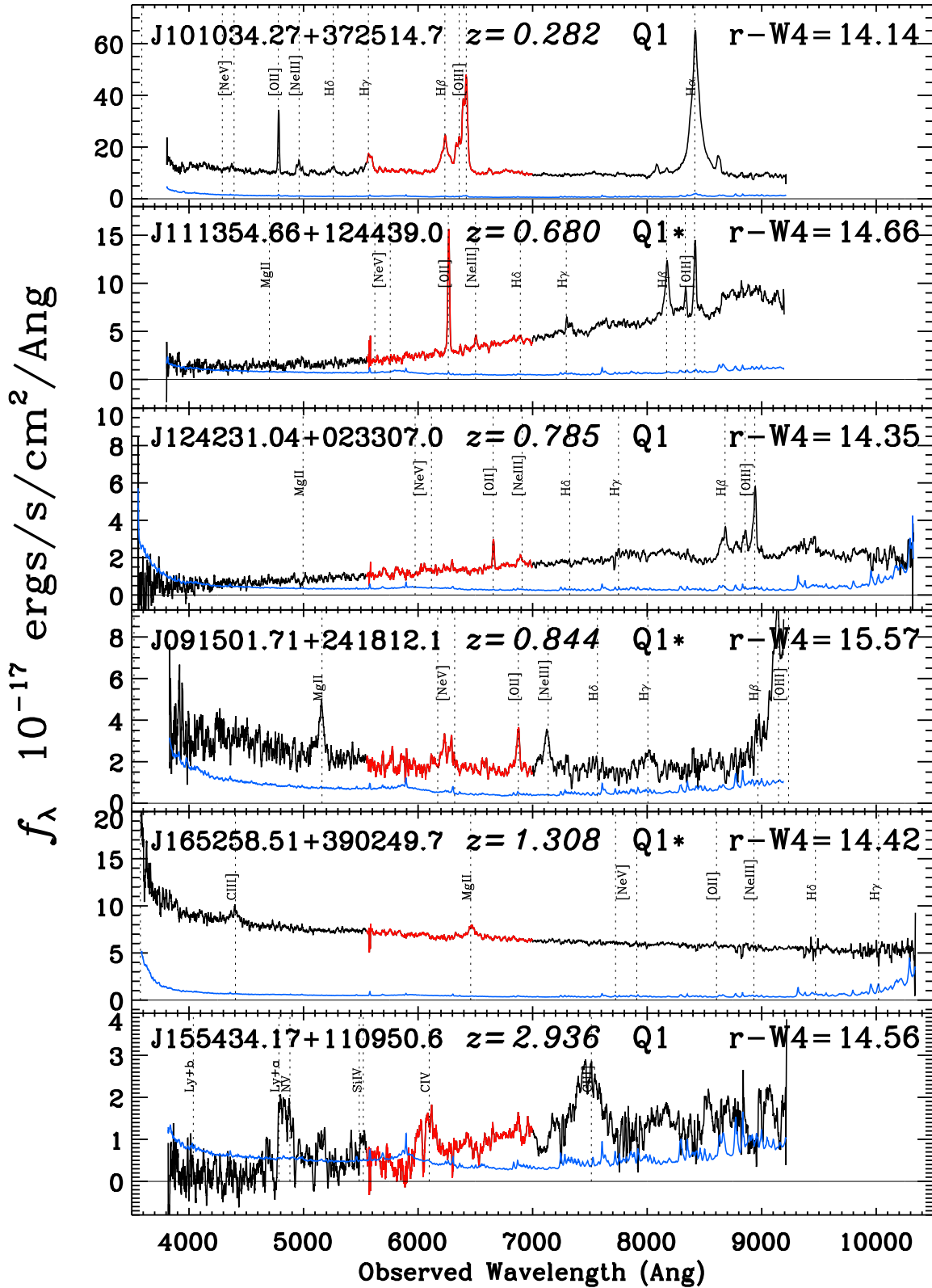


Figure 5. Examples of extremely red quasars classified as Type 1 quasars based on their optical spectroscopy. The SDSS name, redshift, classification and $r - W4$ colour are given in each panel. The red part of the spectrum marks the contribution to the observed r -band flux, while the blue line is the estimated error per pixel (Lee et al. 2013). The spectra are smoothed using an 8-pixel boxcar average. Prominent emission lines often seen in AGN spectra; Ly β 1025.72, Ly α 1215.67, N v 1240.14, Si iv 1393.76, 1402.77, C iv 1548.19, 1550.76 C iii] 1908.73, Mg ii 2798.75 Ne v 3346.82, 3426.84 [O ii] 3728.48 [Ne iii] 3869.85, H δ 4102.89, H γ 4341.68, H β 4862.68, [O iii] 4960.30, 5008.24 and H α 6564.61 \AA , are marked by the vertical dashed lines, where we use vacuum wavelengths for identifying emission lines. Spectra that cut off at 3800 \AA and 9200 \AA are SDSS spectra, while BOSS spectra extend to 3600 \AA and 10,400 \AA . Objects with starred classifications were targeted due to their radio properties.

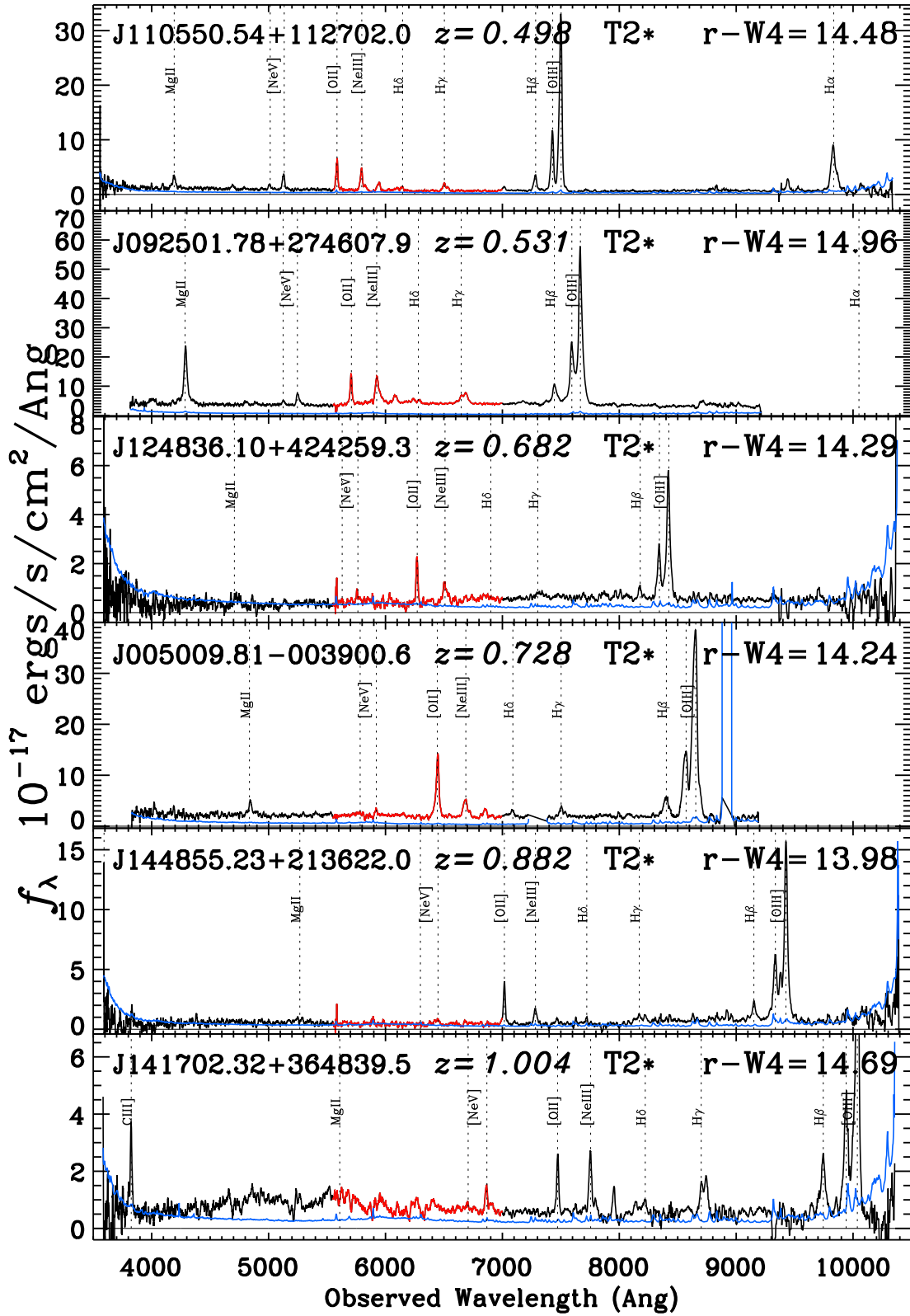


Figure 6. Same as for Fig 5, except showing examples of extremely red quasars classified as Type 2 quasars based on their optical spectroscopy, at $z \lesssim 1.1$.

the broad-line region is completely blocked from the observer by strong obscuration ($A_V > 10$), and nuclear activity is inferred indirectly via the emission line ratios of ionized gas which should be characteristic of photo-ionization by the quasar (Baldwin et al. 1981; Veilleux & Osterbrock 1987). At low redshifts, where $H\beta$ is accessible in the optical spectrum, we can define “Type 2” objects as those in which the kinematic structure of the permitted emission lines is similar to that of the forbidden lines; the permitted lines should not display an additional broad ($\text{FWHM} \gtrsim 2000 \text{ km sec}^{-1}$) component. We also require $[\text{O III}] / H\beta > 3$.

Figure 6 presents examples of Type 2 quasar candidates at $z \lesssim 1$. No line-fitting has been performed, but all objects in this class are seen by visual inspection to have the same kinematics in the permitted $H\beta$ and forbidden $[\text{O III}]$ lines. In the extremely red quasar sample, the quasar nature of the Type 2 candidates is not in doubt: the typical values of $[\text{O III}] / H\beta$ are 10 or greater, and high-ionization species such as $[\text{Ne V}]$ are detected in most cases. However, $H\beta$ can be pretty weak and there may be broad components in some $H\alpha$ lines (Zakamska et al. in prep) which we currently do not have access to.

Among the 29 objects with $z < 1.1$, 20 (69%) are classified as Type 2 active nuclei candidates from their optical spectra; see Figure 6. This high fraction of Type 2 objects is completely uncharacteristic of the parent sample of the SDSS/BOSS quasars, making it clear that the selection based on high infrared-to-optical colours can indeed recover obscured quasars. All seven Type 2 quasars in our sample that were observed before July 2006 are found in the catalog of Reyes et al. (2008).

4.3 Type 2 Quasars candidates at high redshift

At high redshift ($z > 1.5$) we also find objects that have narrow emission lines, weak continua and satisfy the definition of Type 2 candidates; see Figure 7. Although the classifications are performed by visual inspection of the optical spectra, with one exception (noted below) all objects in this class have $\text{FWHM}(\text{C IV}) \lesssim 2000 \text{ km s}^{-1}$.

These objects have similar optical spectra to those described in Yan et al. (2013) and Alexandroff et al. (2013), although there are no objects in common between our sample and that presented in Alexandroff et al. (2013). Those authors present a sample of 145 candidate Type 2 quasars from BOSS at redshifts between 2 and 4.3, using data from DR9 (Ahn et al. 2012). These objects are characterized by weak continuum in the rest-frame ultraviolet with a typical continuum magnitude of $i \approx 22$ (i.e., $M_i(z = 2.5) \approx -25$) and strong lines of C IV and $\text{Ly}\alpha$, with $\text{FWHM} \leq 2000 \text{ km s}^{-1}$. Typical ($\sim L^*$) galaxies are ≥ 1 magnitudes fainter at these redshifts (Marchesini et al. 2007, 2012), suggesting host-galaxy light is not fully sufficient to explain the continuum luminosity and some level of AGN light is getting through/around the absorber.

The reddest quasar in Alexandroff et al. (2013) has $r - W4 = 13.30$. In general, our selection of Type 2 candidates is not as strict as that of Alexandroff et al. (2013), and we classify one object as a Type 2 with $z > 2$, that is in DR9 but not in the Alexandroff et al. (2013) sample; J083448.48+015921.1 at $z = 2.594$ has $\text{FWHM}(\text{C IV})$

$= 2864 \pm 73 \text{ km s}^{-1}$ which is above the 2000 km s^{-1} limit of the Alexandroff et al sample.

While this class of object shows only narrow emission lines in the rest-frame UV spectra, Greene et al. (2014) obtained near-infrared spectroscopy for a subset of the Alexandroff et al. (2013) sample, demonstrating that the $H\alpha$ emission line consistently requires a broad component. This result implies that the typical extinction in these objects is $A_V \lesssim$ a few, sufficient to block the rest-frame UV continuum and broad lines but not the rest-frame optical - consistent with the (relatively) bright continuum.

4.4 Objects with (post-)starburst signatures

Our sample includes quasars that have starburst or post-starburst signatures in their optical spectra. Examples are given in Figure 8. Objects are placed into the starburst class if they exhibit evidence of obvious $[\text{O II}]$ emission, especially when compared with $[\text{O III}]$ (Kennicutt 1998; Kewley & Dopita 2002; Kewley et al. 2004; Moustakas et al. 2006; Mostek et al. 2012). The post-starburst objects are objects which have either a Balmer break, and/or an obvious Balmer series.

Post-starburst quasars exhibit a Balmer edge originating from an A-star population that is not dominated by blue light from OB-stellar populations. Quasars with post-starbursting signatures have been identified previously, (e.g., Brotherton et al. 1999, 2002; Cales et al. 2014) and Cales et al. (2013) derive physical properties from optical spectra while Wei et al. (2013) study the MIR spectral properties of post-starburst quasars.

Considerable study has been carried out using the $[\text{O II}] \lambda 3727\text{\AA}$ forbidden-line doublet and $[\text{O II}]/[\text{O III}]$ ratio as a starburst indicator in AGN and galaxies (e.g., Kauffmann et al. 2003; Groves et al. 2006). The $r - W4 > 14$ quasars that have a starburst signature are some of our most luminous $W4$ -sources; three (out of 5) of our objects have $F_{[W4]} > 50 \text{ mJy}$ (J101034.27+372514.7 top panel of Fig 5; J0941000.8+143614.4 and J111354.66+124439.0 in Fig. 8.)

The quasar J112657.76+163912.0 (hereafter J1126+1639) may have other optical objects within the $W4$ -beam, as we mentioned in Section 2.2. J1126+1639 appears to be at the center of a group/small cluster of other optically red galaxies. However, the other group members are *blue* in $(W1 - W2)$ colour, suggesting that these objects are not bright in $W4$. Our likely candidate appears disturbed in the SDSS optical image, suggesting that it hosts an ongoing merger.

4.5 Broad Absorption Line Quasars

Our $r - W4 > 14$ quasar selection also finds broad absorption line (BAL) objects (Figure 9). From visual inspection of their optical spectra, all objects in this class are obvious strong absorption systems. Although we do not use it for our classifications, the C IV balnicity index (BI; Weymann et al. 1991) for our extremely red BAL quasars as reported in the DR10Q catalog is generally $\log_{10}(\text{BI}_{\text{C IV}}) \gtrsim 3$.

It has been known for some time that BALs can be redder (in optical-to-near infrared colour) than the general quasar population e.g., Hall et al. (1997). Hall et al.

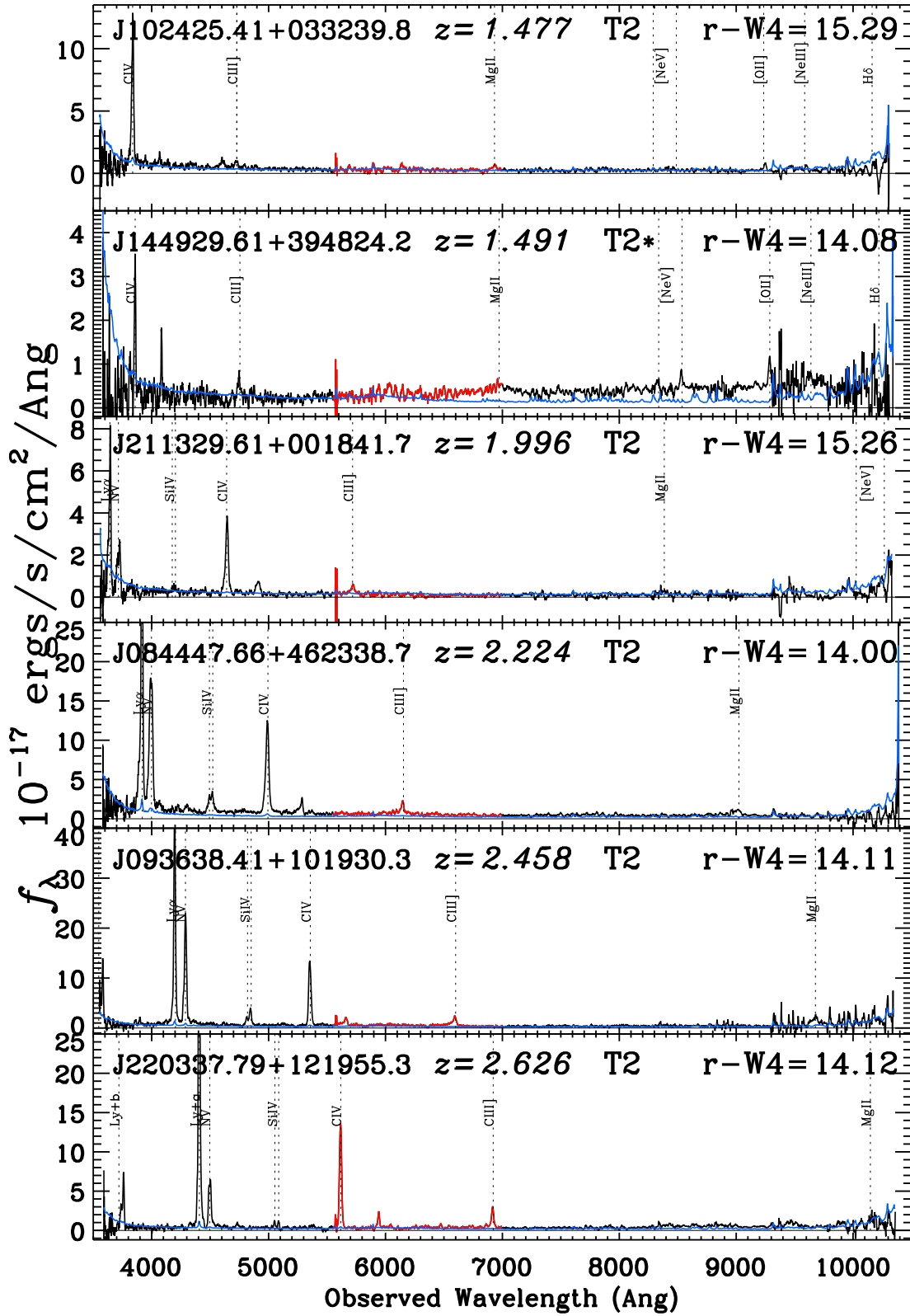


Figure 7. Same as for Fig 5, except showing examples of extremely red quasars classified as Type 2 quasars based on their optical spectroscopy, at $z \gtrsim 1.5$.

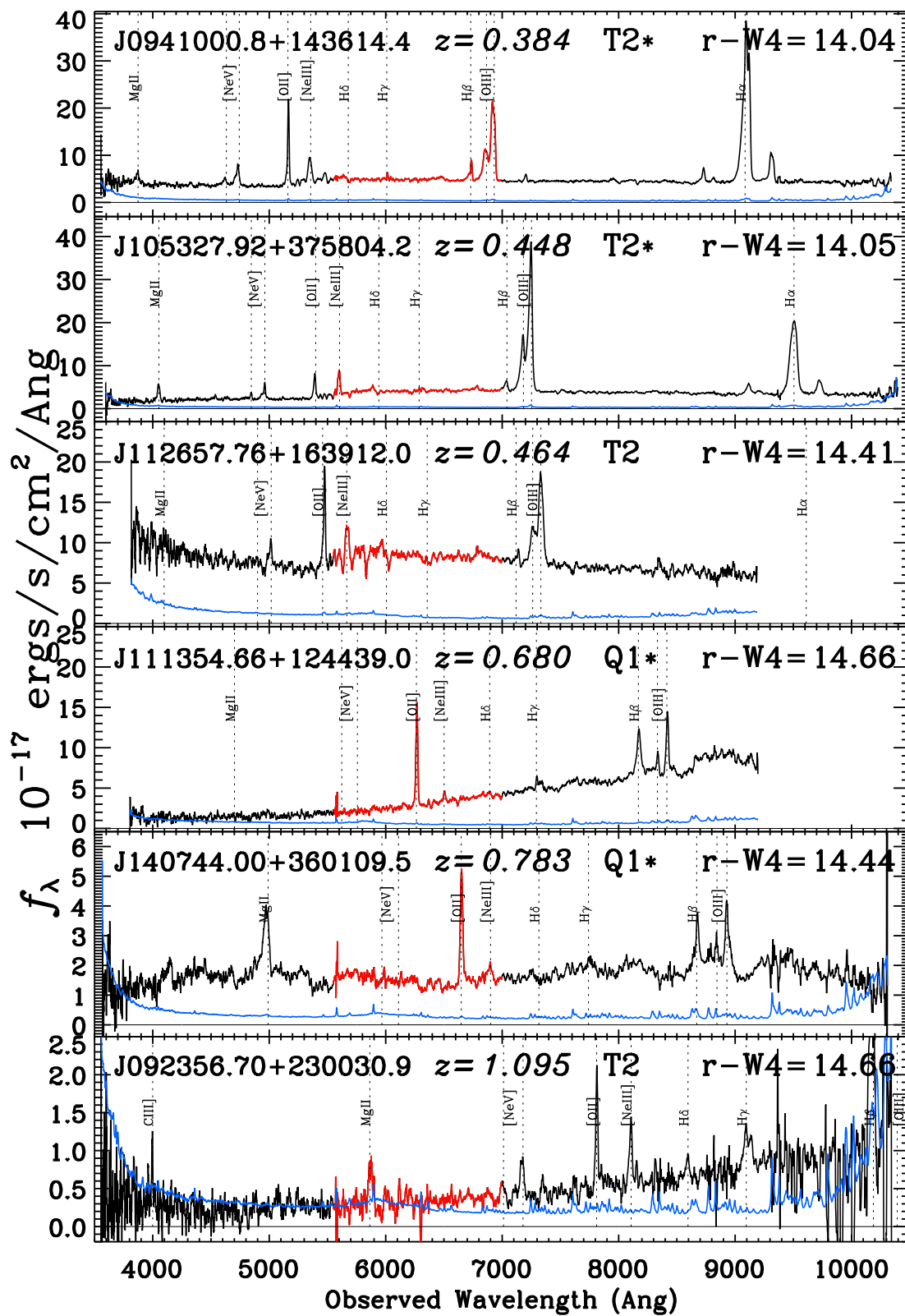


Figure 8. Same as for Fig 5, except showing examples of extremely red quasars that display signatures of an ongoing, or post, star-bursting phase. In particular we identify the Balmer edge in J105327.92+375804.2 and J112657.76+163912.0.

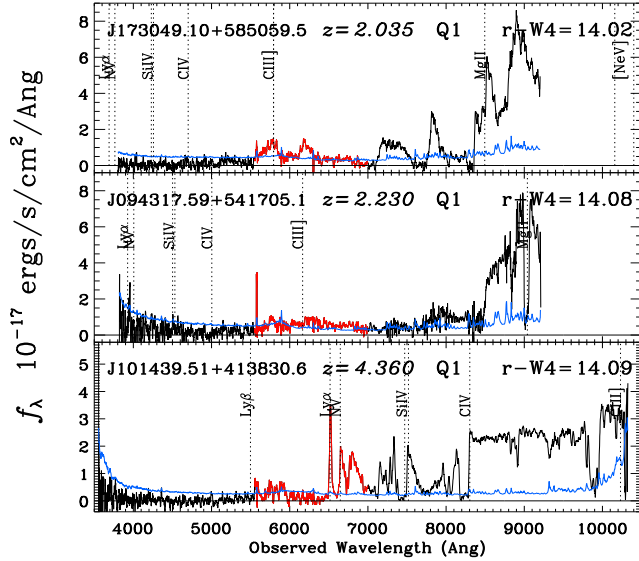


Figure 9. Same as for Fig 5, except showing examples of the Broad Absorption Line quasars, with these three objects being examples of the rarer subclass of FeLoBALs. At $z = 4.36$, J101439.51+413830.6 is the highest redshift object in our full sample.

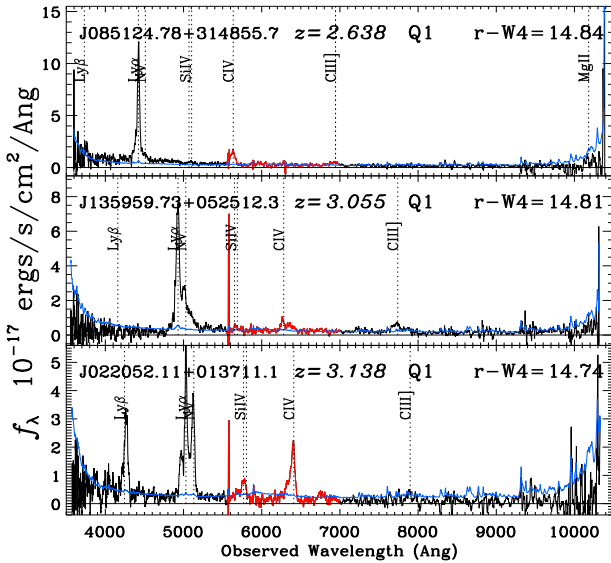


Figure 10. Same as for Fig 5, except showing quasars that are “W1W2-dropouts”. The feature at 5575\AA is the [O I] bright sky line.

(2002) report on a number of heavily-reddened, extreme BAL quasars discovered in SDSS, while Trump et al. (2006), Gibson et al. (2009) and Allen et al. (2011) explore this reddening-BAL relation. However, we note that the presence of the BAL objects do not appear in our sample due to dust reddening; in these objects, the BAL troughs remove a large fraction of the continuum that would otherwise contribute to the r -band flux, which makes the $r - W4$ color even redder.

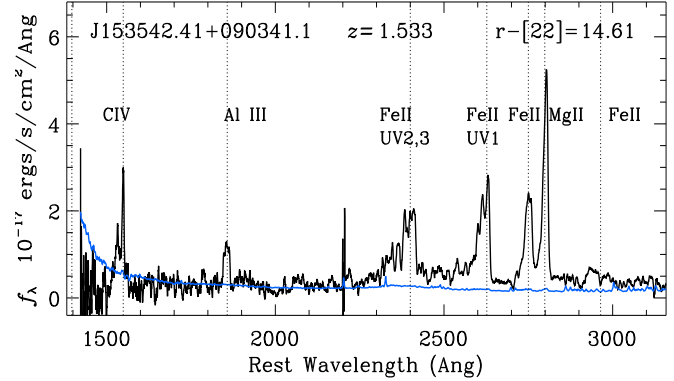


Figure 11. The spectrum of SDSS J153542.41+090341.1. This object has exceptionally strong FeII emission in the UV1 (2600\AA), UV2/3 (2400\AA) and 2740\AA complexes with weak emission from other FeII features.

4.6 W1W2-dropout Quasars

Objects that are selected to be bright at 12 or $22\mu\text{m}$, but undetected by WISE at 3.4 and $4.6\mu\text{m}$ are “W1W2-dropouts”. Eisenhardt et al. (2012) find ~ 1000 such objects over the whole sky, including the $z = 2.452$ source WISE J181417.29+341224.9, a hyper-luminous infrared galaxy (HyLIRG) with $L_{\text{IR}} > 10^{13} L_{\odot}$. WISE 1814+3412 has a $W4$ flux density of $14.38 \pm 0.87 \text{ mJy}$; a $350\mu\text{m}$ detection (Wu et al. 2012) implies a minimum bolometric luminosity of $3.7 \times 10^{13} L_{\odot}$ suggesting the W1W2-dropouts are extreme cases of luminous, hot ($60\text{--}120\text{K}$) dust-obscured galaxies possibly representing a short evolutionary phase during galaxy merging and evolution.

Three of our 65 objects ($\sim 5\%$) satisfy the W1W2-dropout selection criteria. Their optical spectra are shown in Figure 10. These three quasars were all discovered by BOSS, have r -band fluxes of $\approx 5 - 8 \mu\text{Jy}$ (cf., $2.25 \pm 0.11 \mu\text{Jy}$ for WISE 1814+3412) and redshifts $z = 2.638 - 3.138$ placing them in the HyLIRG regime.

Comparing our quasar W1W2-dropouts to the hyper-luminous infrared galaxy population will offer clues linking intense star-formation and high-luminosity accretion activity. We speculate that these are a transition class of quasar, bridging the gap from unreddened “Type 1s” to the recently discovered (Banerji et al. 2013, 2014) heavily reddened/obscured “Type 2” hyper-luminous quasars at high redshift.

4.7 J153542.41+090341.1

Figure 11 displays the spectrum of SDSS J153542.41+090341.1, hereafter J1535+0903, a remarkable object with a unique pattern of emission lines. We classify this quasar as a Type 2 candidate based on line widths in both C IV (Table 2) and Mg II ($\text{FWHM} = 1600 \pm 60 \text{ km s}^{-1}$). However, the exceptionally strong emission in Al III 1860 and in Fe II at $\sim 2300 - 2770\text{\AA}$ point to high densities indicative of a broad line region and thus a Type 1 classification. In particular, photoionization models by Baldwin et al. (1996) demonstrate that large ratios of Al III 1860 compared to the inter-combination lines with similar ionizations, C III] 1909 and especially Si III] 1892 , require densities $n_e \gtrsim 10^{12}$

cm^{-3} . Similarly, Baldwin et al. (2004) showed that this peculiar pattern of FeII emission lines, dominated by a few spikes that include the resonance multiplets UV1 and UV 2,3, also requires densities $\gtrsim 10^{12} \text{ cm}^{-3}$ in a gas with very low ionization parameter. Hamann et al. (in prep.) present a quantitative analysis of this object.

4.8 Extreme Equivalent Width Objects

The EREW objects that we present in Figure 12 all have C IV FWHM $> 2000 \text{ km s}^{-1}$ (Table 2) and are thus classified as Type 1 quasars. These six examples are a set of objects at $z \simeq 2-3$ which are characterized by extreme rest-frame equivalent widths (EREWs) of $\gtrsim 150 \text{ \AA}$ (the measured REWs from the C IV line are given in Fig. 12). For comparison, typical quasars have $\text{REW}(\text{C IV}) \approx 25-50 \text{ \AA}$ (Figure 13). This sample includes six broad-line sources with $\text{REW}(\text{C IV}) \gtrsim 150 \text{ \AA}$, of which four have $\text{REW}(\text{C IV}) > 200 \text{ \AA}$. Some of the extreme REW sources also have unusual line properties including: unusually high $\text{N V}/\text{Ly}\alpha$, enhanced $\text{Si IV}+\text{O IV}$ and weak He II and C III]. Some also have strong $\text{Ly}\beta$ and unusual $\text{Ly}\alpha$ profiles.

Figure 13 displays the distribution of C IV rest equivalent widths in the BOSS DR10 Quasar catalog. This plot uses line data from the DR10Q catalog, and selects sources that have: $2.0 < z < 3.4$, the visual inspection flag for BALs set to 0 (i.e. no BALs), $\text{FWHM}(\text{C IV}) > 2000 \text{ km s}^{-1}$, and the ratio of the C IV rest-frame equivalent width to its uncertainty to be > 3 . A total of 98807 quasars satisfy these criteria and in the cumulative distribution, 5.8% of quasars have $\text{REW}(\text{C IV}) > 100 \text{ \AA}$ with 1.3% having $\text{REW}(\text{C IV}) > 150 \text{ \AA}$. This is to be compared to 55% (45%) of the non-BAL Type 1s with measurable C IV in our sample having $\text{REW}(\text{C IV}) > 100$ (150) \AA .

J1535+0903 (Section 4.7) may also be a member of this class. We measure $\text{REW}(\text{C IV}) \approx 136 \text{ \AA}$, and $\text{REW}(\text{Mg II})$ is $\sim 280 \text{ \AA}$, depending on uncertain continuum placement. This source shares a strong Al III 1860 line with the $\text{N V}/\text{Ly}\alpha > 1$ objects.

The large REWs in these objects might be caused by suppressed continuum emission analogous to Type 2 quasars in the Unified Model. However, the large line widths (e.g., compared to typical narrow line regions Liu et al. (2013)) and in some cases very high densities (Hamann et al., in prep.) suggest that the line-emitting regions are close to the central continuum source, like typical broad line regions. It therefore seems difficult to have dust obscuring the continuum source without also obscuring the broad emission lines. We note we are not testing or contradicting the Unified Model. However, *if* we interpret the large REWs as due to continuum obscuration, then a simple unified picture e.g., Urry & Padovani (1995) where when there is continuum obscuration, there is also obscuration of the BLR and a Type 2 quasar is observed, does not fully explain these objects. Other possibilities to explain the physical nature of the EREW quasars include spatially extended broad line regions, chance alignments of dusty clumps in a clumpy torus, and highly-ionized gas in a failed BAL wind or a thick accretion disk corona directly above the continuum-emitting disk. Unusual emission line ratios in some of the EREW quasars, including $\text{NV } \lambda 1240$ stronger than $\text{Ly}\alpha$ and an unusual pattern of FeII lines at 2300–2770 \AA , suggest that un-

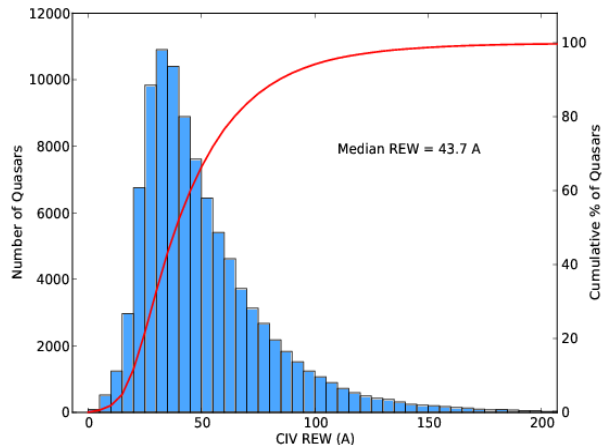


Figure 13. The distribution of C IV rest equivalent widths in the BOSS DR10 Quasar catalog (blue histogram). The red curve is the cumulative distribution.

usual physical conditions in the broad emission line regions are sometimes involved. We investigate these issues further in Hamann et al. (2014, in prep.).

5 SUMMARY AND CONCLUSIONS

We have matched the quasar catalogs of the SDSS and BOSS with WISE to identify quasars with extremely high infrared-to-optical ratios $r_{\text{AB}} - W4_{\text{Vega}} > 14 \text{ mag}$ (i.e., $F_{\nu}(22\mu\text{m})/F_{\nu}(r) \gtrsim 1000$). We identify 65 objects and note the following findings and conclusions:

- This sample spans a redshift range of $0.28 < z < 4.36$ with a median of $z \sim 1.5$.
- We recover a broad range of quasar spectrum in this selection. The majority of the objects have spectra of reddened Type 1 quasars, Type 2 quasars (both at low and high redshift) and objects with strong absorption features.
- There is a high fraction of Type 2 objects at low redshift, suggesting that a high optical-to-infrared colour can be an efficient selection of narrow-line quasars.
- There are three objects that are detected in the W4-band but not W1 or W2 (i.e., “W1W2-dropouts”) all of which are at $z > 2.6$.
- We identify an intriguing class of objects at $z \simeq 2-3$ which are characterized by equivalent widths of $\text{REW}(\text{C IV}) \gtrsim 150 \text{ \AA}$. These objects often also have unusual line properties. We speculate that the large REWs may be caused by suppressed continuum emission analogous to Type 2 quasars in the Unified Model. However, there is no obvious mechanism in the Unified Model to suppress the continuum without also suppressing the broad emission lines, thus potentially providing an interesting challenge to quasar models.

ACKNOWLEDGEMENTS

We thank R. M. Cutri and the IPAC team for the “Explanatory Supplement” to the WISE All-Sky and AllWISE Data Release Products resource. Peregrine McGehee and the IRSA HelpDesk were also very useful. AllWISE makes use of data from WISE, which is a joint project of the University of California, Los Angeles, and the Jet Propulsion

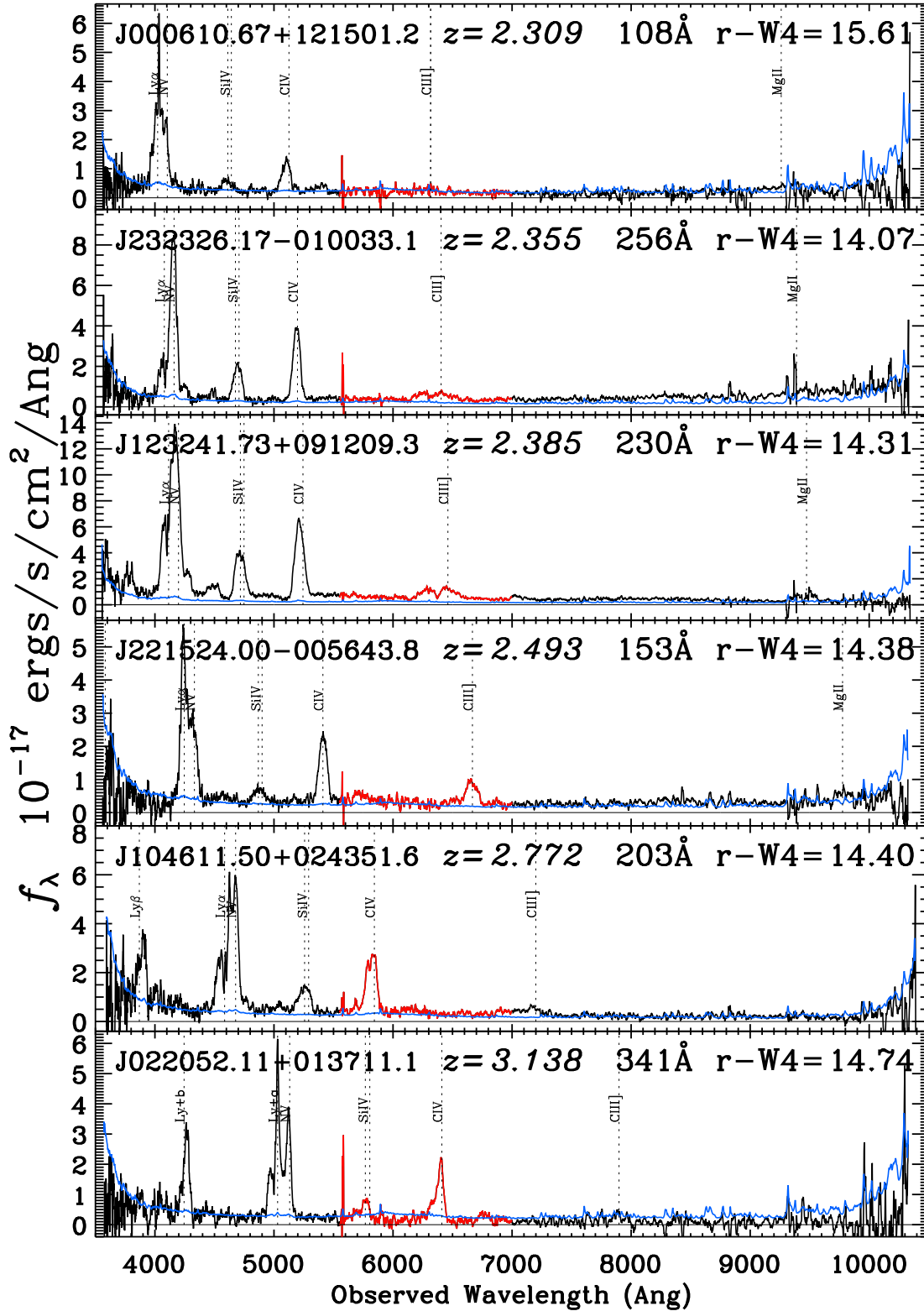


Figure 12. Same as for Fig 5, except showing examples of the new set of “Extreme Rest-frame Equivalent Width” (REWE) objects. These objects possess large REWs of e.g. the CIV line (values given in Table 2), unusual profiles of the Ly α /NV complex (and the ratio of Ly α :NV) and flat continua in all examples. The quasar J022052.11+013711.1 (bottom panel) is also a W1W2-dropout (Fig. 10).

Laboratory/California Institute of Technology, and NEO-WISE, which is a project of the Jet Propulsion Laboratory/California Institute of Technology. WISE and NEO-WISE are funded by the National Aeronautics and Space Administration. This research made use of the NASA Astrophysics Data System. The data and code used herein will become publicly available at upon publication of the paper. N.P.R acknowledges that funding for part of this project was supplied by NASA and the *Hubble* Grant Number: HST-GO-13014.06. FH acknowledges support from the USA National Science Foundation grant AST-1009628.

Funding for SDSS-III has been provided by the Alfred P. Sloan Foundation, the Participating Institutions, the National Science Foundation, and the U.S. Department of Energy. The SDSS-III web site is <http://www.sdss3.org/>. SDSS-III is managed by the Astrophysical Research Consortium for the Participating Institutions of the SDSS-III Collaboration including the University of Arizona, the Brazilian Participation Group, Brookhaven National Laboratory, University of Cambridge, University of Florida, the French Participation Group, the German Participation Group, the Instituto de Astrofísica de Canarias, the Michigan State/Notre Dame/JINA Participation Group, Johns Hopkins University, Lawrence Berkeley National Laboratory, Max Planck Institute for Astrophysics, New Mexico State University, New York University, Ohio State University, Pennsylvania State University, University of Portsmouth, Princeton University, the Spanish Participation Group, University of Tokyo, University of Utah, Vanderbilt University, University of Virginia, University of Washington, and Yale University. *Facilities: SDSS, WISE*

REFERENCES

- Abazajian K. N., et al., 2009, *ApJS*, 182, 543
 Ahn C. P., et al., 2012, *ApJS*, 203, 21
 Ahn C. P., et al., 2014, *ApJS*, 211, 17
 Alexander D. M., Hickox R. C., 2012, *NewAR*, 56, 93
 Alexandroff R., Strauss M. A., et al., 2013, *MNRAS*, 423, 1325
 Allen J. T., Hewett P. C., Maddox N., Richards G. T., Belokurov V., 2011, *MNRAS*, 410, 860
 Antonucci R., 1993, *ARA&A*, 31, 473
 Antonucci R. R. J., Miller J. S., 1985, *ApJ*, 297, 621
 Assef R. J., et al., 2013, *ApJ*, 772, 26
 Baldwin J. A., Ferland G. J., Korista K. T., Carswell R. F., Hamann F., Phillips M. M., Verner D., Wilkes B. J., Williams R. E., 1996, *ApJ*, 461, 664
 Baldwin J. A., Ferland G. J., Korista K. T., Hamann F., LaCluyzé A., 2004, *ApJ*, 615, 610
 Baldwin J. A., Phillips M. M., Terlevich R., 1981, *PASP*, 93, 5
 Banerji M., Fabian A. C., McMahon R. G., 2014, *MNRAS*
 Banerji M., McMahon R. G., Hewett P. C., Gonzalez-Solares E., Kuposov S. E., 2013, *MNRAS*, 429, L55
 Becker R. H., White R. L., Helfand D. J., 1995, *ApJ*, 450, 559
 Bolton A. S., et al., 2012, *AJ*, 144, 144
 Brandt W. N., Hasinger G., 2005, *ARA&A*, 43, 827
 Brotherton M. S., et al., 1999, *ApJ Lett.*, 520, L87
 Brotherton M. S., Grabelsky M., Canalizo G., van Breugel W., Filippenko A. V., Croom S., Boyle B., Shanks T., 2002, *PASP*, 114, 593
 Cales S., Brotherton M. S., Shang Z., Bennert V., Canalizo G., Diamond-Stanic A. M., 2014 Vol. 223 of *AAS*, #115.06
 Cales S. L., et al., 2013, *ApJ*, 762, 90
 Chiu K., Richards G. T., Hewett P. C., Maddox N., 2007, *MNRAS*, 375, 1180
 Cutri R. M., et al., 2011, Technical report, Explanatory Supplement to the WISE Preliminary Data Release Products
 Dawson K., et al., 2013, *AJ*, 145, 10
 Dey A., et al., 2008, *ApJ*, 677, 943
 Diamond-Stanic A. M., Rieke G. H., 2010, *ApJ*, 724, 140
 Donley J. L., et al., 2012, *ApJ*, 748, 142
 Draine B. T., Li A., 2007, *ApJ*, 657, 810
 Eisenhardt P. R. M., et al., 2012, *ApJ*, 755, 173
 Eisenstein D. J., Weinberg D. H., et al., 2011, *AJ*, 142, 72
 Elitzur M., 2008, *NewAR*, 52, 274
 Elvis M., 2010, in *IAU Symposium Vol. 267, The Quasar Continuum*. pp 55–64
 Elvis M., et al., 1994, *ApJS*, 95, 1
 Fabian A. C., 2012, *ARA&A*, 50, 455
 Fukugita M., Ichikawa T., Gunn J. E., Doi M., Shimasaku K., Schneider D. P., 1996, *AJ*, 111, 1748
 Fynbo J. P. U., Krogager J.-K., Venemans B., Noterdaeme P., Vestergaard M., Møller P., Ledoux C., Geier S., 2013, *ApJS*, 204, 6
 Gibson R. R., et al., 2009, *ApJ*, 692, 758
 Glikman E., et al., 2012, *ApJ*, 757, 51
 Glikman E., et al., 2013, *ApJ*, 778, 127
 Glikman E., Gregg M. D., Lacy M., Helfand D. J., Becker R. H., White R. L., 2004, *ApJ*, 607, 60
 Glikman E., Helfand D. J., White R. L., Becker R. H., Gregg M. D., Lacy M., 2007, *ApJ*, 667, 673
 Greene J. E., et al., 2014, *ApJ* submitted
 Groves B. A., Heckman T. M., Kauffmann G., 2006, *MNRAS*, 371, 1559
 Gunn J. E., et al., 1998, *AJ*, 116, 3040
 Gunn J. E., et al., 2006, *AJ*, 131, 2332
 Hall P. B., et al., 2002, *ApJS*, 141, 267
 Hall P. B., Martini P., Depoy D. L., Gatley I., 1997, *ApJ Lett.*, 484, L17
 Heckman T., Best P., 2014, *ArXiv:1403.4620v1*
 Hopkins P. F., et al., 2005, *ApJ*, 630, 705
 Hopkins P. F., et al., 2006, *ApJS*, 163, 1
 Hopkins P. F., Richards G. T., Hernquist L., 2007, *ApJ*, 654, 731
 Jurek R. J., Drinkwater M. J., Francis P. J., Pimblett K. A., 2008, *MNRAS*, 383, 673
 Kauffmann G., et al., 2003, *MNRAS*, 346, 1055
 Kennicutt Jr. R. C., 1998, *ARA&A*, 36, 189
 Kewley L. J., Dopita M. A., 2002, *ApJS*, 142, 35
 Kewley L. J., Geller M. J., Jansen R. A., 2004, *AJ*, 127, 2002
 Khachikian E. Y., Weedman D. W., 1974, *ApJ*, 192, 581
 Kirkpatrick J. D., et al., 2011, *ApJS*, 197, 19
 Krawczyk C. M., Richards G. T., Mehta S. S., Vogeley M. S., Gallagher S. C., Leighly K. M., Ross N. P., Schneider D. P., 2013, *ApJS*, 206, 4
 Lacy M., et al., 2004, *ApJS*, 154, 166
 Lawrence A., et al., 2007, *MNRAS*, 379, 1599

- Lee K.-G., et al., 2013, *AJ*, 145, 69
- Lidz A., Hopkins P. F., Cox T. J., Hernquist L., Robertson B., 2006, *ApJ*, 641, 41
- Liu G., Zakamska N. L., Greene J. E., Nesvadba N. P. H., Liu X., 2013, *MNRAS*, 436, 2576
- Maddox N., Hewett P. C., Péroux C., Nestor D. B., Wisotzki L., 2012, *MNRAS*, 424, 2876
- Maddox N., Hewett P. C., Warren S. J., Croom S. M., 2008, *MNRAS*, 386, 1605
- Mainzer A., et al., 2011, *ApJ*, 731, 55
- Marchesini D., et al., 2007, *ApJ*, 656, 42
- Marchesini D., Stefanon M., Brammer G. B., Whitaker K. E., 2012, *ApJ*, 748, 126
- Martínez-Sansigre A., Rawlings S., Lacy M., Fadda D., Jarvis M. J., Marleau F. R., Simpson C., Willott C. J., 2006, *MNRAS*, 370, 1479
- Mostek N., Coil A. L., Moustakas J., Salim S., Weiner B. J., 2012, *ApJ*, 746, 124
- Moustakas J., Kennicutt Jr. R. C., Tremonti C. A., 2006, *ApJ*, 642, 775
- Myers A. D., Brunner R. J., Nichol R. C., Richards G. T., Schneider D. P., Bahcall N. A., 2007, *ApJ*, 658, 85
- Myers A. D., et al., 2006, *ApJ*, 638, 622
- Nakos T., et al., 2009, *Astron. & Astrophys.*, 494, 579
- Norman C., et al., 2002, *ApJ*, 571, 218
- Oke J. B., Gunn J. E., 1983, *ApJ*, 266, 713
- Pâris I., et al., 2014, *Astron. & Astrophys.*, 563, A54
- Peth M. A., Ross N. P., Schneider D. P., 2011, *AJ*, 141, 105
- Polletta A., et al., 2008, *ApJ*, 675, 960
- Reyes R., et al., 2008, *AJ*, 136, 2373
- Richards G. T., et al., 2002, *AJ*, 123, 2945
- Richards G. T., et al., 2003, *AJ*, 126, 1131
- Richards G. T., et al., 2006a, *ApJS*, 166, 470
- Richards G. T., et al., 2006b, *AJ*, 131, 2766
- Richards G. T., et al., 2009, *AJ*, 137, 3884
- Ross N. P., et al., 2009, *ApJ*, 697, 1634
- Ross N. P., et al., 2012, *ApJS*, 199, 3
- Ross N. P., et al., 2013, *ApJ*, 773, 14
- Sanders D. B., Soifer B. T., Elias J. H., Madore B. F., Matthews K., Neugebauer G., Scoville N. Z., 1988, *ApJ*, 325, 74
- Schlegel D. J., Finkbeiner D. P., Davis M., 1998, *ApJ*, 500, 525
- Schneider D. P., et al., 2010, *AJ*, 139, 2360
- Shen Y., 2009, *ApJ*, 704, 89
- Shen Y., et al., 2009, *ApJ*, 697, 1656
- Shen Y., et al., 2011, *ApJS*, 194, 45
- Smee S. A., et al., 2013, *AJ*, 146, 32
- Smith J. A., et al., 2002, *AJ*, 123, 2121
- Souchay J., et al., 2009, *Astron. & Astrophys.*, 494, 799
- Stern D., et al., 2002, *ApJ*, 568, 71
- Stern D., et al., 2005, *ApJ*, 631, 163
- Stern D., et al., 2012, *ApJ*, 753, 30
- Stoughton C., et al., 2002, *AJ*, 123, 485
- Trump J. R., et al., 2006, *ApJS*, 165, 1
- Urrutia T., Lacy M., Becker R. H., 2008, *ApJ*, 674, 80
- Urry C. M., Padovani P., 1995, *PASP*, 107, 803
- Vanden Berk D. E., et al., 2001, *AJ*, 122, 549
- Veilleux S., Osterbrock D. E., 1987, *ApJS*, 63, 295
- Wei P., Shang Z., Brotherton M. S., Cales S. L., Hines D. C., Dale D. A., Ganguly R., Canalizo G., 2013, *ApJ*, 772, 28
- Weymann R. J., Morris S. L., Foltz C. B., Hewett P. C., 1991, *ApJ*, 373, 23
- White M., et al., 2012, *MNRAS*, 999, 126
- Wright E. L., et al., 2010, *AJ*, 140, 1868
- Wu J., et al., 2012, *ApJ*, 756, 96
- Wu X., Jia Z., 2010, *MNRAS*, 406, 1583
- Wu X.-B., Wang R., Schmidt K. B., Bian F., Jiang L., Fan X., 2011, *AJ*, 142, 78
- Wu X.-B., Zuo W., Yang J., Yang Q., Wang F., 2013, *AJ*, 146, 100
- Yan L., et al., 2013, *AJ*, 145, 55
- York D. G., et al., 2000, *AJ*, 120, 1579
- Zakamska N. L., et al., 2003, *AJ*, 126, 2125